ISSN 1674-1056
http://cpb.iphy.ac.cn
http://iopscience.iop.org/cpb
中国物理 B
Chinese Physics
中国物理 Chinese Physics B

Unidirectional rotation of circles driven by chiral active particles

Jiamin Chen(陈佳敏), Xiaolin Zhou(周晓琳), Linxi Zhang(章林溪)

Citation: Chin. Phys. B . 2018, 27(11): 118701. **doi:** 10.1088/1674-1056/27/11/118701
Journal homepage: http://cpb.iphy.ac.cn; http://iopscience.iop.org/cpb

What follows is a list of articles you may be interested in

A network of conformational transitions in an unfolding process of HP-35 revealed by high-temperature MD simulation and a Markov state model

Dandan Shao(邵丹丹), Kaifu Gao(高恺夫)
Chin. Phys. B . 2018, 27(1): 018701. **doi:** 10.1088/1674-1056/27/1/018701

Molecular dynamic simulation of the thermodynamic and kinetic properties of nucleotide base pair

Yu-Jie Wang(王宇杰), Zhen Wang(王珍), Yan-Li Wang(王晏莉), Wen-Bing Zhang(张文炳)
Chin. Phys. B . 2017, 26(12): 128705. **doi:** 10.1088/1674-1056/26/12/128705

Anisotropic formation mechanism and nanomechanics for the self-assembly process of cross-*β* peptides

Li Deng(邓礼), Yurong Zhao(赵玉荣), Peng Zhou(周鹏), Hai Xu(徐海), Yanting Wang(王延颋)
Chin. Phys. B . 2017, 26(12): 128701. **doi:** 10.1088/1674-1056/26/12/128701

Combined effects of headgroup charge and tail unsaturation of lipids on lateral organization and diffusion of lipids in model biomembranes

Xiao-Jie Chen(陈晓洁), Qing Liang(梁清)
Chin. Phys. B . 2017, 26(4): 048701. **doi:** 10.1088/1674-1056/26/4/048701

Modulation of intra- and inter-sheet interactions in short peptide self-assembly by acetonitrile in aqueous solution

Li Deng(邓礼), Yurong Zhao(赵玉荣), Peng Zhou(周鹏), Hai Xu(徐海), Yanting Wang(王延颋)
Chin. Phys. B . 2016, 25(12): 128704. **doi:** 10.1088/1674-1056/25/12/128704

Unidirectional rotation of circles driven by chiral active particles*

Jiamin Chen(陈佳敏), Xiaolin Zhou(周晓琳), and Linxi Zhang(章林溪)†

Department of Physics, Zhejiang University, Hangzhou 310027, *China*

(Received 21 June 2018; revised manuscript received 3 September 2018; published online 25 October 2018)

The dynamics of two-dimensional rigid circles filled with chiral active particles are investigated by employing the overdamped Langevin dynamics simulations. Unidirectional rotation of rigid circles is observed, and the rotational angular velocity (ω') relies mainly on the length (l), the number (n_B), and tilt angle (γ) of boards, and the angular velocity (ω) and area fraction (ρ) of chiral active particles. There are optimum values for these parameters at which the average angular velocity of circle reaches its maximum. The center-of-mass mean square displacement for circles drops by about two orders of magnitude for large angular velocity ω of chiral active particles with oscillations in the short-time regime. Our work demonstrates that nanofabricated objects with suitable designs immersed in a bath of chiral active particles can extract and rectify energy in a unidirectional motion.

Keywords: unidirectional rotation, dynamics, chiral active particle, nanofabricated object

PACS: 87.10.Tf, 87.85.St, 87.85.Va **DOI:** 10.1088/1674-1056/27/11/118701

1. Introduction

Active Brownian motions are frequently found in nature, with examples ranging from microorganisms such as bacteria and Eukaryotic cells to macroscopic entities such as bird flocks and mammals herds.[1–4] Like living organisms, active Brownian particles are able to propel themselves into directed motion in the absence of external drives because they have the ability to extract energy from an external source and convert it to motility.[5,6] Hence, active particles, also referred to as self-propelled particles, hold tremendous potential applications; e.g., drug delivery within tissues,[7,8] gene therapy,[9] nanoscale assembly,[10,11] and pollution management.[12] However, sometimes active particles are asymmetric so that the driving force and propulsion direction are no longer aligned, resulting in circular motion with a well-defined chirality.[13–15] The methods that lead to chiral motion may be diverse; e.g., magnetic fields and optical tweezers.[16,17] Actually, many biological organisms can spin naturally, such as clusters of sperm cells and dancing algae.[18,19] In another example, *E. coli* bacteria trace out circular trajectories when moving near a surface.[20]

Biological systems usually move in confined structures, such as membranes and intracellular space. More recently, confinements are known to have profound effects on active systems; for instance, target search,[21] ratchet transport,[22] phase separation,[23,24] long lived density fluctuation,[25] and formation of spiral vortex.[26] There are a variety of confining structures, which can be roughly classified into two types: flexible boundaries and rigid walls. The case of deformable boundaries enclosing active particles has been recently investigated, in which shape and displacement fluctuations are analyzed theoretically and numerically.[27–30] In addition, the case of rigid boundaries[21,26,31–37] is also a hot topic over the past several years, especially for nanofabricated objects immersed in active particles.[33–35] These studies draw a conclusion that an asymmetric gear can rectify random motion of self-propelled particles, which, in return, exert a torque on the gear and drive it into unidirectional motion.[33–35] In this paper, we consider chiral active particles constrained by a rigid circle which is grafted with four boards regularly. In contrast from previous studies, the rotary gear with symmetric teeth can exhibit unidirectional motion in our systems due to the asymmetry of the chiral active particles. The aim of this work is to investigate how to improve the rotation efficiency of circles by adjusting the structure of rigid circles. Our results can provide insight into the design of nanofabricated objects such as molecular motors, which can extract energy and translate it into mechanical motion in out-of-equilibrium environment.

2. Model and methods

We perform two-dimensional simulations to investigate the dynamical behaviors of rigid circles filled with N chiral active particles. The rigid circle is modeled as a ring of L colloidal beads grafted with n_B boards regularly (n_B is the number of boards). Each board consisting of l beads is grafted on the ring with a tilt angle γ. The diameters of the chiral active particles and beads of rigid circles are uniformly σ. The chiral active particles have a translational velocity V_0 for self-propulsion and an angular velocity ω for self-rotation in a counterclockwise direction. The dynamics of the i-th chiral active particle is described by the position $\boldsymbol{r}_i$ of its center and the orientation θ_i of the polar axis $\boldsymbol{u}_i = (\cos\theta_i, \sin\theta_i)$, obeying

*Project supported by the National Natural Science Foundation of China (Grant Nos. 21674096 and 21873082).

†Corresponding author. E-mail: lxzhang@zju.edu.cn

© 2018 Chinese Physical Society and IOP Publishing Ltd

the following overdamped Langevin equations:[22,30,31,38]

$$\partial_t \boldsymbol{r}_i = V_0 \boldsymbol{u}_i - \mu \nabla_i U + \sqrt{2D_0}\xi_i^{\mathrm{T}}(t), \quad (1)$$

$$\partial_t \theta_i = \omega + \sqrt{2D_\theta}\xi_i^{\mathrm{R}}(t), \quad (2)$$

where μ is the mobility and U is the configurational energy. $\xi_i^{\mathrm{T}}(t)$ and $\xi_i^{\mathrm{R}}(t)$ are Gaussian white noise with zero mean and satisfy $\langle \xi_{i\alpha}^{\mathrm{T}}(t)\xi_{j\beta}^{\mathrm{T}}(s)\rangle = \delta_{ij}\delta_{\alpha\beta}\delta(t-s)(\alpha,\beta = x,y)$ and $\langle \xi_i^{\mathrm{R}}(t)\xi_j^{\mathrm{R}}(s)\rangle = \delta_{ij}\delta(t-s)$, respectively.[39] $\langle\cdots\rangle$ donates an ensemble average over the distribution of the noise, and δ is the Dirac delta function. D_0 and D_θ denote the translational and rotational diffusion coefficients, respectively. The relations of $\mu = D_0/k_{\mathrm{B}}T$ and $D_\theta = 3D_0/\sigma^2$ can be found. The area fraction of the chiral active particles in rigid circle is defined by $\rho = N\sigma^2/(4R_0^2)$, where R_0 corresponds to the radius of the circle given explicitly by $R_0 = (2\sin(\pi/L))^{-1}\sigma$.[30] Here, we neglect the little area of boards for simplicity.

The interactions between two chiral active particles or between the active particle and bead of rigid circle are represented by a purely repulsive truncated and shifted Lennard–Jones potential[40]

$$U_{\mathrm{LJ}}(r) = \begin{cases} 4\varepsilon\left[\left(\dfrac{\sigma}{r}\right)^{12} - \left(\dfrac{\sigma}{r}\right)^{6}\right] + \dfrac{1}{4}, & r < 2^{1/6}\sigma, \\ 0, & r \geq 2^{1/6}\sigma, \end{cases} \quad (3)$$

where r is the distance between any two particles (or particle-bead), and $\varepsilon = k_{\mathrm{B}}T$.

Molecular dynamics (MD) simulations are carried out by performing Langevin dynamics with the open source software, LAMMPS,[41] and all the simulation snapshots are captured using the visual molecular dynamics (VMD) package.[42] The rigid circle driven by chiral active particles can wander in the x–y plane of $(200\sigma)^2$ with periodic boundary conditions. The equations of motion can be converted into dimensionless forms by using σ and ε as basic units of length and energy, and $\tau_0 = \sigma^2/D_0$ as the unit of time.[23] The time step is chosen to be $\tau = 0.0001\tau_0$, and the total simulation time for each run is more than 2×10^8 τ. Meanwhile, the parameters are set to be $D_0 = 0.01$, $D_\theta = 0.03$, $\mu = 0.01$, $L = 120$, and $V_0 = 0.5$. We have performed the simulations with various angular velocities of chiral active particles from $\omega = 0$ to 1.0, and various area fractions of active particles from $\rho = 0.05$ to 0.6. Moreover, the parameters of boards such as board length l and tilt angle γ as well as the number of boards n_{B} are changed to study their effects.

3. Results and discussion

3.1. Unidirectional rotation of circles

In previous studies, we know that asymmetric objects immersed in a bath of self-propelled bacteria exhibit a unidirectional motion.[33–35] For example, a specially designed flexible object was found to rotate unidirectionally driven by active particles due to spontaneous symmetry breaking.[43] Here, the rigid circles with symmetric boards ($\gamma = \pi/2$) filled with chiral active particles can also lead to a unidirectional motion. Unlike the self-propelled particles, the direction of motion and that of the force of chiral active particles are no longer aligned, which can induce a circular motion.[13–15,38] Therefore, the collision between chiral active particles and rigid circle can also result in the asymmetry properties.

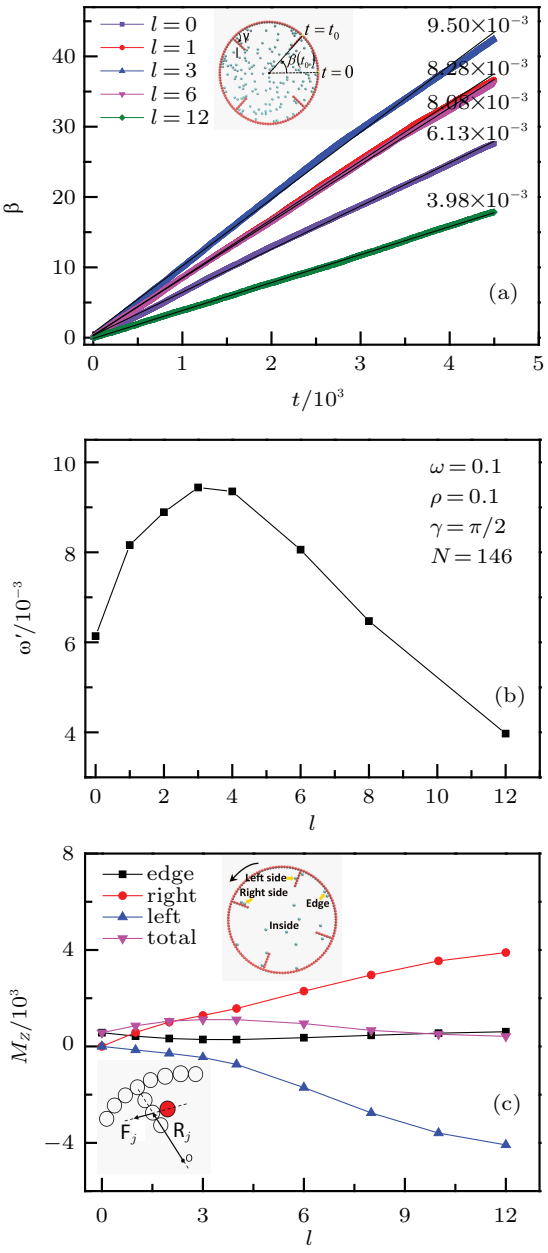


Fig. 1. (color online) (a) Cumulative rotation angle β of a rigid circle as a function of time t for various board lengths l. The inset figure is a schematic illustration of the rotation angle $\beta(t_0)$ at time t_0, and the straight black lines are linear fitting curves. (b) The corresponding relationship between average angular velocity ω' of a rigid circle and board length l. Here the angular velocity ω of chiral active particles is 0.1, the area fraction ρ is 0.1, the number of boards n_{B} is 4, and the tilt angle γ of boards is $\pi/2$. (c) Resultant moment M_Z of rigid circle suffered from the collision of active particles on various collision positions. The inset figures show the division of collision positions and the definition of M_Z.

Figure 1 shows the rotation motion of rigid circles driven by chiral active particles with various board lengths from $l = 0$

to 12 at a fixed angular velocity of chiral active particle of $\omega = 0.1$. Here, the area fraction ρ of chiral active particles is 0.1, the total number of chiral active particles is $N = 147$, the tilt angle γ of boards is $\pi/2$, and the number of boards is $n_B = 4$. Figure 1(a) presents the time evolution of the cumulative rotation angle β of a rigid circle. The inset figure is a schematic illustration showing the rotation angle $\beta(t_0)$ at time t_0 with counterclockwise direction as the forward direction. In Fig. 1(a), the cumulative rotation angle β increases gradually with time t. The straight black lines are linear fitting curves and the slopes are marked on the upper right. The slope of line increases first and decreases next as the board length increases, displaying a non-monotonic behavior. To understand more clearly this novel behavior in Fig. 1(b), we calculate the average angular velocity ω' of the circle, which is defined as[30]

$$\omega' = \left\langle \lim_{t\to\infty} \frac{\beta(t) - \beta(0)}{t} \right\rangle, \tag{4}$$

where $\langle \cdots \rangle$ represents an ensemble average over 100 runs. We observe a single peak at around $l = 3$, which means that there is an optimum board length for the unidirectional rotation of circle. To find out why the optimum value of board length appears, we measure the resultant moment M_Z of rigid circle, which can be regard as the most important factor affecting the rotation motion, see Fig. 1(c). The inset figure shows the division of collision positions, and there are three collision positions, which may contribute to the rotation motion. Specifically, we calculate the resultant moments M_Z originating from the edge of circle, the right-hand and left-hand sides of boards, respectively. The lower left-hand figure is a schematic illustration of calculating the moment of force, and the resultant moment M_Z is defined as

$$M_Z = \left\langle \sum_{j=1}^{Q} \boldsymbol{R}_j \times \boldsymbol{F}_j \right\rangle, \tag{5}$$

where $\boldsymbol{R}_j$ refers to the position of bead relative to the center of mass of rigid circle, and $\boldsymbol{F}_j$ donates the force on bead from a collision. Since we calculate the M_Z of three collision positions respectively, Q means the total number of collisions for one position, such as the right side at a certain moment. In addition, $\langle \cdots \rangle$ represents an ensemble average over all conformations. Apparently, the moment of force generated by the collision on the right-hand side of the boards is always positive as the driving moment. Correspondingly, the moment of force on the left-hand side of the boards can prove to be the moment of resistance. In accordance with our previous work, the collision angle between active particles and the boundary is inclined to be less than $\pi/2$ because of the counterclockwise circular motion ($\omega > 0$) for chiral active particles.[30] Consequently, the resultant moment M_Z from the collision on the edge is more likely to be the driving moment. Moreover, we combine these three resultant moments together as the total resultant moment. As shown in Fig. 1(c), as the board length increases, the absolute value of M_Z for the right side (or left side) becomes larger due to the higher collision probability. The value of M_Z of the edge is maintained at a small positive value and slightly changed. The general trend of the total M_Z is consistent with that of ω' in Fig. 1(b), and they have the same optimum board length ($l = 3$).

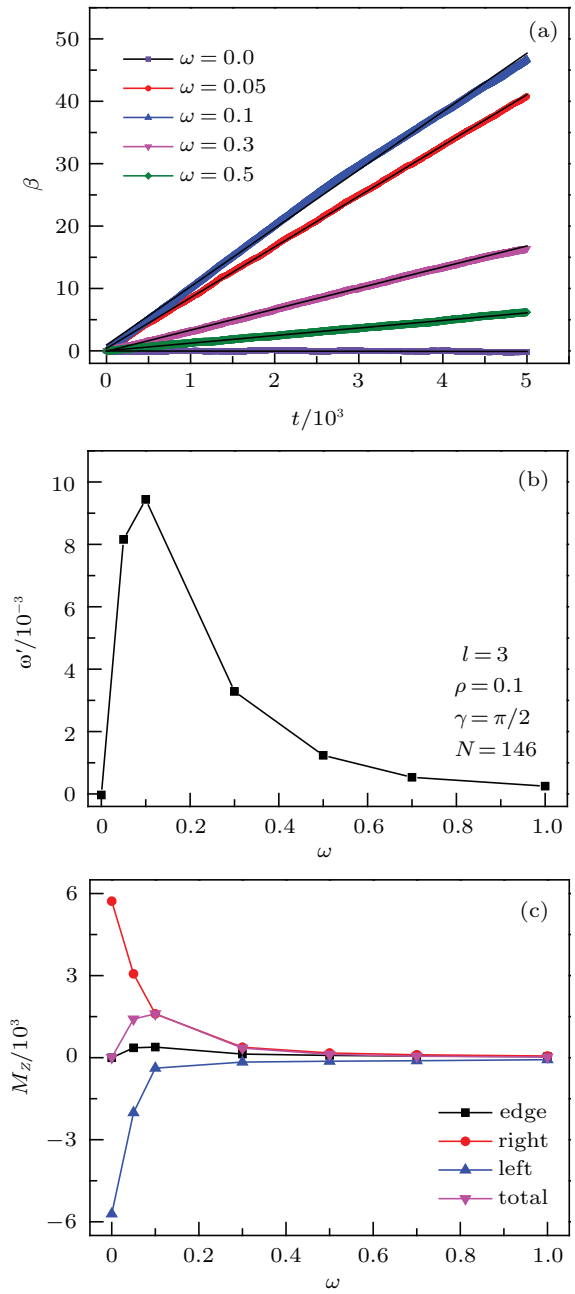


Fig. 2. (color online) (a) Cumulative rotation angle β of a rigid circle as a function of time t for different angular velocities ω of chiral active particles with $l = 3$, $\rho = 0.1$, $n_B = 4$, and $\gamma = \pi/2$. The straight black lines are linear fitting curves. (b) Average angular velocity ω' and (c) resultant moment M_Z of a rigid circle as a function of ω.

In Fig. 2, we display the cumulative rotation angle β as a function of time t for different angular velocities ω of chiral

active particles with parameters of $l = 3$, $\rho = 0.1$, $n_B = 4$, and $\gamma = \pi/2$. Figure 2(a) shows a linear dependence of rotation angle β on time t. For the case of $\omega = 0$, the rotation angle β oscillates near zero, indicating that the circle almost does not rotate with time. This also gives the support to the conclusion that symmetric gear diffuses with no preferred direction of motion under the impacts of self-propelled robots.[35] Besides, there is obviously a non-monotonic relationship between the slope of β and the angular velocity ω. As shown in Fig. 2(b), we observe a sharp increase of average angular velocity ω' before $\omega = 0.1$ followed by a relatively slow decline. And the average angular velocity of rigid circle reaches its maximum ($\omega' = 9.5 \times 10^{-3}$) at $\omega = 0.1$. This non-monotonic behavior is similar to that found by Wu *et al.*, who focused on the rectification of chiral active particles in an asymmetric channel.[36] Figure 2(c) presents the resultant moment M_Z of various collision positions. We can find that absolute values of M_Z for the right and left sides monotonically decrease with ω increasing from 0 to 1.0. This can be attributed to the decreasing collision probability on boards for the decreasing rotation radius of chiral active particles. However, the non-monotonic curve of M_Z for edge cannot be explained by only collision probability. The impact of angular velocity on the edge of circle has been thoroughly discussed in our previous article,[30] which can also be applied here. An extremely low angular velocity ($\omega \approx 0$) results in disorganized collisions on the boundary, although the probability of collisions is large enough. In contrast, the collisions occur rarely for particles with large angular velocity ($\omega = 1.0$) since their trajectories are circular and the radius of circular trajectory is quite small if angular velocity ω is quite large.[36,38] Consequently, there is a moderate angular velocity. Combining these three parts, the curve of total M_Z exhibits an extreme point of $\omega = 0.1$ at which rigid circle rotates counterclockwise with a maximum average angular velocity ω'.

Considering the influence of area fraction ρ of chiral active particles on the rotation motion, we also measure the cumulative rotation angle β as shown in Fig. 3(a). Here, the constants are chosen to be $l = 3$, $\omega = 0.1$, $n_B = 4$, and $\gamma = \pi/2$. At $t = 4.5 \times 10^3$, β increases from 34.8 for $\rho = 0.05$ to 48.9 for $\rho = 0.2$, and then decreases to 34.1 for $\rho = 0.6$. Further research is made in Fig. 3(b), average angular velocity ω' of circle increases before $\rho = 0.2$, reaches a small platform of $\omega' = 1.1 \times 10^{-2}$, and decreases after $\rho = 0.3$. This means that the effects of area fraction here differ from those for soft vesicles in our previous paper, which demonstrate a tendency to increase monotonously with ρ increasing.[30] To investigate the appearance of non-monotonic effect of ρ, we calculate the resultant moment M_Z of rigid circle which is presented in Fig. 3(c). Actually, the absolute values of M_Z for these three positions (edge, right-hand and left-hand sides) will increase monotonously as ρ becomes larger, which can also be explained by the increasing collision probability. When we add these three parts together, however, the total M_Z exhibits a non-monotonic trend. It is easy to understand that a crowded state for chiral active particles will appear when the area fraction ρ approaches to 1.0. Once the chiral active particles in circle become very crowded, their circular motion will not be easily performed. That is to say, chiral active particles will be hard to drive the circles to rotate unidirectionally just like self-propelled particles.

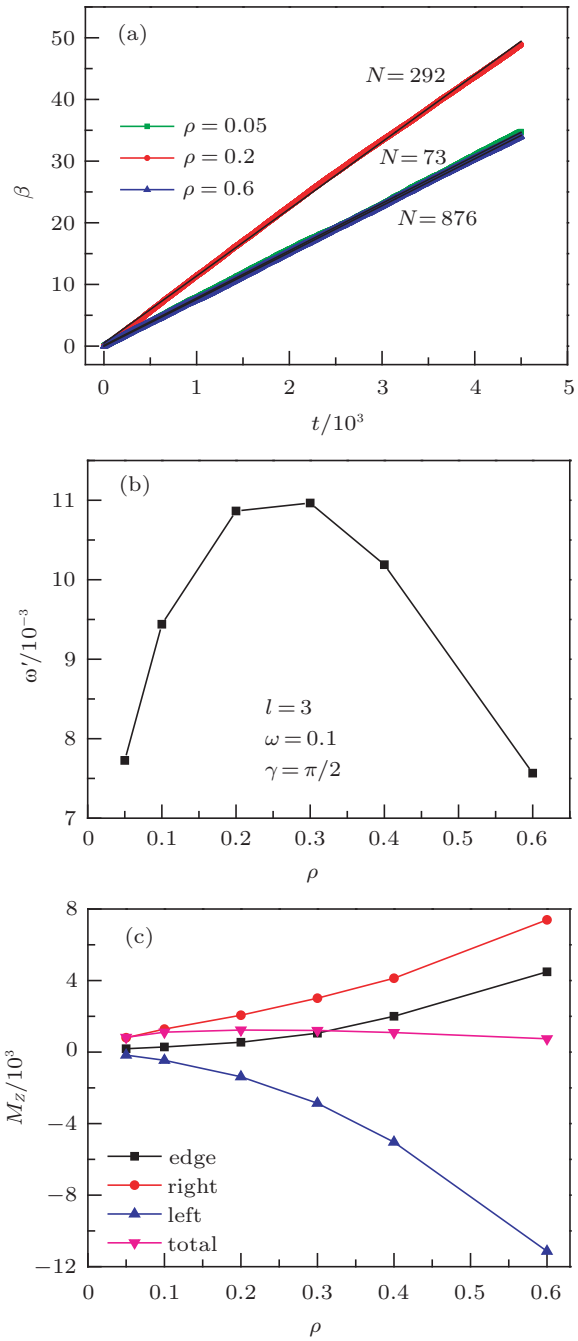


Fig. 3. (color online) (a) Cumulative rotation angle β of a rigid circle as a function of time t for different area fractions ρ of chiral active particles with $l = 3$, $\omega = 0.1$, $n_B = 4$, and $\gamma = \pi/2$. The straight black lines are linear fitting curves. (b) Average angular velocity ω' and (c) resultant moment M_Z of a rigid circle as a function of ρ.

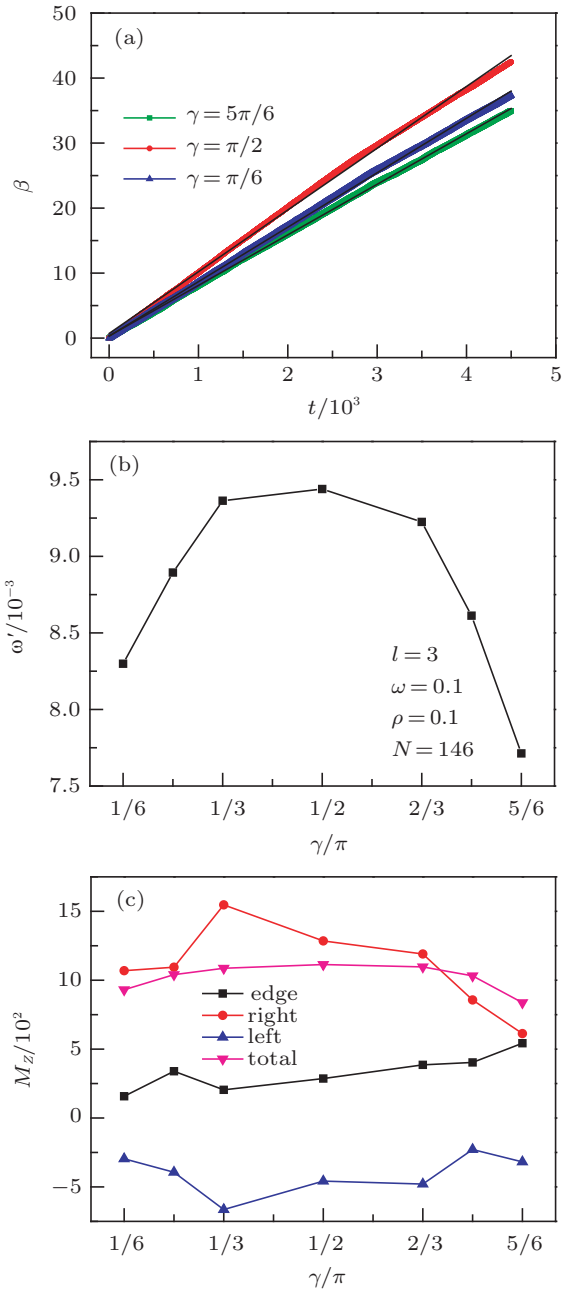


Fig. 4. (color online) (a) Cumulative rotation angle β of a rigid circle as a function of time t for various tilt angles γ of boards with $l = 3$, $\omega = 0.1$, $n_B = 4$, and $\rho = 0.1$. The straight black lines are linear fitting curves. (b) Average angular velocity ω' and (c) resultant moment M_Z of a rigid circle as a function of γ.

To analyze the rotation motion with asymmetric structure of circle in more detail, we change the tilt angle γ of boards, whose definition is already given in the inset of Fig. 1(a). Similarly, we observe a non-monotonic transformation with γ increasing, see Figs. 4(a) and 4(b). Furthermore, the rotation of circle is a little faster for $\gamma < \pi/2$ compared to their supplementary angles. Here, $l = 3$, $\omega = 0.1$, $n_B = 4$, and $\rho = 0.1$. Figure 4(c) shows the resultant moment M_Z as a function of γ for various collision positions. The total M_Z results from the synergistic reaction of the three parts but the curves of these three parts are complex and irregular with the change of γ. Although the cause is the difference in collision probability from different positions, we try to explain it in a more intuitive way. As γ increases from $\pi/6$ to $5\pi/6$, the number of active particles captured by the right space of boards increases first and then decreases. Of course, the capture of particles is temporary in our simulations, the particles will still go somewhere else after a while. In contrast to their supplementary angles, the tilt angle less than $\pi/2$ is easier to capture chiral active particles and keeps them stay longer. We can think of the case that the result will be completely opposite if the rotation of chiral active particles is set to be clockwise. That is to say, the tilt angle ($\gamma > \pi/2$) is more conducive to rotation motion for clockwise active particles, and then the rigid circle will rotate clockwise.

We also take into account the effects of number of boards (n_B) on the rotations of circles, and the results are shown in Fig. 5. For example, in Fig. 5, at $t = 4.5 \times 10^3$, β increases from 42.5 for $n_B = 4$ to 46.7 for $n_B = 6$, and then still increases to 51.9 for $n_B = 12$. The inset figure displays the average angular velocity ω' of rigid circle as a function of the number of boards n_B with parameters of $l = 3$, $\rho = 0.1$, $\omega = 0.1$, and $\gamma = \pi/2$. The average angular velocity ω' increases monotonically with n_B increasing from 0 to 15, however, the growth rate is slowly decreasing for large n_B.

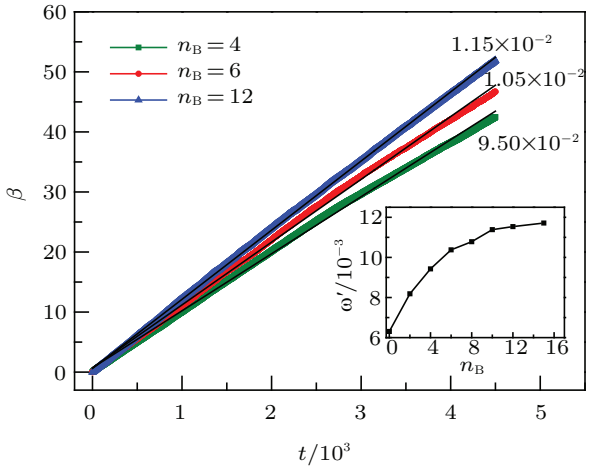


Fig. 5. (color online) Cumulative rotation angle β of a rigid circle as a function of time t for various number of boards (n_B) with $l = 3$, $\rho = 0.1$, $\omega = 0.1$, and $\gamma = \pi/2$. The inset figure displays the average angular velocity ω' of rigid circle with different number of boards n_B.

3.2. Diffusion of circles

Apart from the unidirectional rotation of circles, we study the diffusion of rigid circles filled with chiral active particles in Fig. 6. Here, the parameters are chosen as $l = 3$, $\rho = 0.1$, $n_B = 4$, and $\gamma = \pi/2$. The mean square displacement $g_3(t)$ of the rigid circles filled with chiral active particles is defined as[44]

$$g_3(t) = \langle (x_{cm}(t) - x_{cm}(0))^2 + (y_{cm}(t) - y_{cm}(0))^2 \rangle, \quad (6)$$

where $x_{cm}(t)$ and $y_{cm}(t)$ are the coordinates of the center of mass of the system composed of rigid circle and active particles, respectively. As shown in Fig. 6(a), there are three curves

of $g_3(t)$ for various angular velocity ω of chiral active particles. For $\omega = 0$, we observe a superdiffusion of circles at short time,[21] followed by a normal diffusion at long time. As for $\omega = 0.5$ and $\omega = 1.0$, the curves display oscillations in the short-time regime with the amplitude fading as time goes by. Figure 6(b) is an enlarged figure at short timescales, and the oscillation period is in accordance with the rotation period of active particles; that is, the oscillation originates from the circular rotation of chiral active particles.

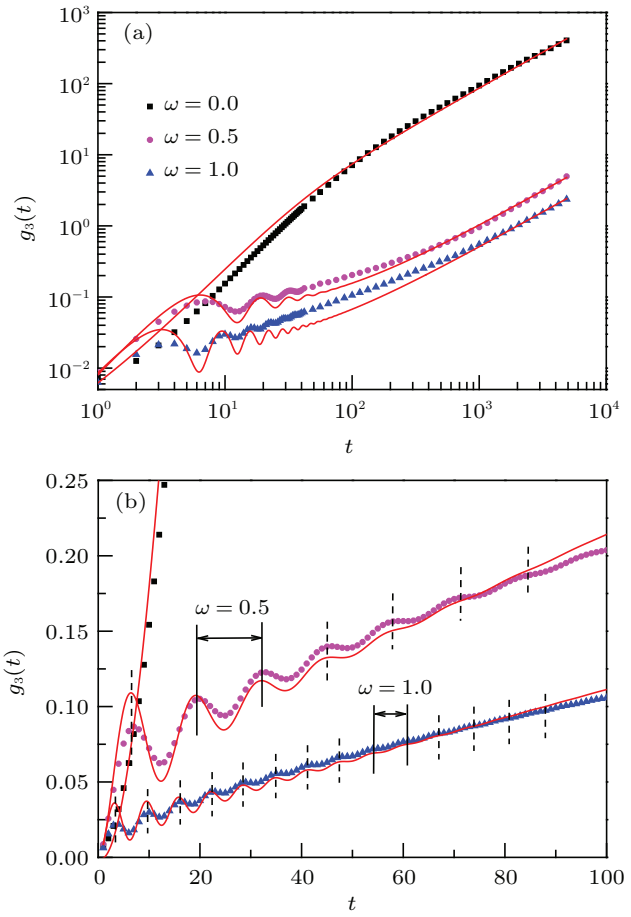


Fig. 6. (color online) Mean square displacement $g_3(t)$ of the center of mass of system for different angular velocities with an area fraction of $\rho = 0.1$. Here $l = 3$, $n_B = 4$, and $\gamma = \pi/2$. Solid red lines are fitting curves based on Eq. (7) with the parameter of $D = 2.19 \times 10^{-2}$, $A = 1.40$ for $\omega = 0$ (black symbols), $D = 2.42 \times 10^{-4}$, $A = 5.99 \times 10^{-2}$ for $\omega = 0.5$ (pink symbols), and $D = 1.23 \times 10^{-4}$, $A = 1.82 \times 10^{-2}$ for $\omega = 1.0$ (blue symbols). (b) The enlarged figure of the front part of (a) shows that the oscillation period of the curve is consistent with the rotation period of chiral active particles, and the amplitude of oscillation decreases gradually with time t.

Going back to Fig. 6(a), the $g_3(t)$ drops about two orders of magnitude as the angular velocity becomes large for active particles. We can deduce that $g_3(t)$ approaches zero if angular velocity ω tends to infinity because the radius of circular trajectory is extremely small and chiral active particles prefer to rotate around their own center. Solid red lines are fitting curves based on the following equation:

$$g_3(t) = 4Dt + A[e^{-2D_\theta t}\cos(\omega t + \phi_0) - \cos\phi_0]. \quad (7)$$

In contrast to the formula derivation in our previous manuscript,[30] both D and A are fitting parameters. The two models are distinct because soft vesicle is replaced by rigid ring grafted by several boards. We substitute $2D_\theta$ for D_θ just as some literatures do[15,38] because it is more suitable for the fitting of the data here. Besides, $\cos\varphi_0$ is given by[30]

$$\cos\phi_0 = \frac{D_\theta^2 - \omega^2}{D_\theta^2 + \omega^2}. \quad (8)$$

The overall trend of red fitting lines is consistent with the simulation data, except for some positions. Therefore, it is necessary to research deeply to rectify Eq. (7) for various confining structures in future studies and try to find out the exact coefficients, such as D and A.

4. Concluding remarks

Active particles with proper designs are able to convert energy into expected applications. Accordingly, the designed circles can extract and rectify energy from chiral active particles into unidirectional motion, which can be used in plenty of fields such as molecular motors in biology.[45,46] In this paper, we investigated numerically the system of chiral active particles confined in rigid circle which is grafted with some boards regularly. We observed unidirectional motion of rigid circles driven by chiral active particles under the influence of length l, tilt angle γ, and number of boards n_B, and angular velocity ω and area fraction ρ of active particles. The appearance of non-monotonic curves indicates that there are optimum values for these parameters. To explain this phenomenon, we measured the resultant moment M_Z of rigid circles for various collision positions. Moreover, the center-of-mass mean square displacement for circles drops about two orders of magnitude for large angular velocity ω of chiral active particles with oscillations in the short-time regime. Our results can provide some designs for nanofabricated objects immersed in a bath of chiral active particles and achieve better regulation of its unidirectional rotation.

References

[1] Vicsek T and Zafeiris A 2012 *Phys. Rep.* **517** 71
[2] Peruani F, Starruß J, Jakovljevic V and Bär M 2012 *Phys. Rev. Lett.* **108** 098102
[3] Cavagna A and Giardina I 2014 *Annu. Rev. Condens. Matter Phys.* **5** 183
[4] Gueron S, Levin S A and Rubenstein D I 1996 *J. Theor. Biol.* **182** 85
[5] Purcell E M 1977 *Am. J. Phys.* **45** 3
[6] Erdmann U, Ebeling W, Schimansky-Geier and Schweitzer F 2000 *Eur. Phys. J. B* **15** 105
[7] Ford R M and Harvey R W 2007 *Adv. Water Res.* **30** 1608
[8] Chen J X, Chen Y G and Ma Y Q 2016 *Soft Matter* **12** 1876
[9] Yang W, Misko V R, Nelissen K, Kong M and Peeters F M 2012 *Soft Matter* **8** 5175
[10] Ghosh A and Fischer P 2009 *Nano Lett.* **9** 2243
[11] Ezhilan B, Gao W, Pei A, *et al.* 2015 *Nanoscale* **7** 7833
[12] Chin C D, Linder V and Sia S K 2007 *Lab Chip* **7** 41
[13] Teeffelen S and Löwen H 2008 *Phys. Rev. E* **78** 020101
[14] Mijalkov M and Volpe G 2013 *Soft Matter* **9** 6376

[15] Sevilla F J 2016 *Phys. Rev. E* **94** 062120
[16] Grzybowski B A and Whitesides G M 2002 *Science* **296** 718
[17] Grier D G 1997 *Curr. Opin. Colloid Interface Sci.* **2** 264
[18] Riedel I H, Kruse K and Howard J 2005 *Science* **309** 300
[19] Drescher K, Leptos K C, Tuval I, *et al.* 2009 *Phys. Rev. Lett.* **102** 168101
[20] Lauga E, DiLuzio W R, Whitesides G M and Stone H A 2006 *Biophys. J.* **90** 400
[21] Wang J, Chen Y, Yu W and Luo K 2016 *J. Chem. Phys.* **144** 204702
[22] Ai B Q 2016 *Sci. Rep.* **6** 18740
[23] Redner G S, Hagan M F and Baskaran A 2013 *Phys. Rev. Lett.* **110** 055701
[24] Nguyen N H P, Klotsa D, Engel M and Glotzer S C 2014 *Phys. Rev. Lett.* **112** 075701
[25] Narayan V, Ramaswamy S and Menon N 2007 *Science* **317** 105
[26] Wioland H, Woodhouse F G, Dunkel J, *et al.* 2013 *Phys. Rev. Lett.* **110** 268102
[27] Tian W D, Guo Y K, Chen K and Ma Y Q 2015 *arXiv* 1511.08573
[28] Spellings M, Engel M, Klotsa D, *et al.* 2015 *Proc. Natl. Acad. Sci. USA* **112** E4642
[29] Paoluzzi M, Leonardo R D, Marchetti M C and Angelani L 2016 *Sci. Rep.* **6** 34146
[30] Chen J M, Hua Y F, Jiang Y W and Zhang L X 2017 *Sci. Rep.* **7** 15006
[31] Hua Y F, He L L and Zhang L X 2017 *Chin. Phys. B* **26** 080702
[32] Hua Y F, Li K, Zhou X L, He L L and Zhang L X 2018 *Soft Matter* **14** 5205
[33] Leonardo R D, Angelani L, Arciprete D D, *et al.* 2010 *Proc. Natl. Acad. Sci. USA* **107** 9541
[34] Sokolov A, Apodaca M M, Grzybowski B A and Aranson I S 2010 *Proc. Natl. Acad. Sci. USA* **107** 969
[35] Li H and Zhang H P 2013 *Europhys. Lett.* **102** 50007
[36] Wu J C, Chen Q and Ai B Q 2015 *J. Stat. Mech.* **7** P07005
[37] Deng Z, Zhang D and Zhang L X 2016 *Chin. J. Polym. Sci.* **34** 623
[38] Volpe G, Gigan S and Volpe G 2014 *Am. J. Phys.* **82** 659
[39] Dünweg B and Paul W 1991 *Int. J. Mod. Phys. C* **2** 817
[40] Isele-Holder R E, Elgeti J and Gompper G 2015 *Soft Matter* **11** 7181
[41] Plimpton S 1995 *J. Comput. Phys.* **117** 1
[42] Humphrey W, Dalke A and Schulten K 1996 *J. Mol. Graphics* **14** 33
[43] Li H S, Wang C, Tian W D, *et al.* 2017 *Soft Matter* **13** 8031
[44] Kremer K and Grest G S 1998 *J. Chem. Phys.* **92** 5057
[45] Tafoya S and Bustamante C 2018 *Philos. Trans. Royal Soc. B* **373** 20170181
[46] Kyongwan K, Natsuhiko Y, Sanjib B, *et al.* 2018 *Soft Matter* **14** 3221